Journal of Environmental Sciences 26 (2014) 683–693

Available online at www.sciencedirect.com

Journal of Environmental Sciences

www.jesc.ac.cn

Effects of synthesis methods on the performance of Pt + Rh/$Ce_{0.6}Zr_{0.4}O_2$ three-way catalysts

Zongcheng Zhan, Liyun Song, Xiaojun Liu, Jiao Jiao, Jinzhou Li, Hong He*

Laboratory of Catalysis Chemistry and Nano-Science, Department of Chemistry and Chemical Engineering, College of Environmental and Energy Engineering, Beijing University of Technology, Beijing 100124, China. E-mail: zhanzongcheng@emails.bjut.edu.cn

ARTICLE INFO

Article history:
Received 06 April 2013
revised 18 May 2013
accepted 24 June 2013

Keywords:
UAMR
three way catalyst
Pt and Rh nanoparticles
precipitation
thermal stability
DOI: 10.1016/S1001-0742(13)60444-1

ABSTRACT

The 0.7 wt% Pt + 0.3 wt% Rh/$Ce_{0.6}Zr_{0.4}O_2$ catalysts were fabricated via different methods, including ultrasonic-assisted membrane reduction (UAMR) co-precipitation, UAMR separation precipitation, co-impregnation, and sequential impregnation. The catalysts were physico-chemically characterized by N_2 adsorption, XRD, TEM, and H_2-TPR techniques, and evaluated for three-way catalytic activities with simulated automobile exhaust. UAMR co-precipitation- and UAMR separation precipitation-prepared catalysts exhibited a high surface area and metal dispersion, wide λ window and excellent conversion for NO*x* reduction under lean conditions. Both fresh and aged catalysts from UAMR-precipitation showed the high surface areas of ca. 60–67 m^2/g and 18–22 m^2/g, respectively, high metal dispersion of 41%–55%, and small active particle diameters of 2.1–2.7 nm. When these catalysts were aged, the catalysts prepared by the UAMR method exhibited a wider working window ($\Delta\lambda$ = 0.284–0.287) than impregnated ones ($\Delta\lambda$ = 0.065–0.115) as well as excellent three-way catalytic performance, and showed lower T_{50} (169°C) and T_{90} (195°C) for NO reduction than the aged catalysts from impregnation processes, which were at 265 and 309°C, respectively. This implied that the UAMR-separation precipitation has important potential for industrial applications to improve catalytic performance and thermal stability. The fresh and aged 0.7 wt% Pt + 0.3 wt% Rh/$Ce_{0.6}Zr_{0.4}O_2$ catalysts prepared by the UAMR-separation precipitation method exhibited better catalytic performance than the corresponding catalysts prepared by conventional impregnation routes.

Introduction

Air pollution is known to be the most important environmental issue in modern society. Automobile exhaust gas is the major mobile source of pollution, and the pollutants discharged from automobiles can induce many negative impacts on the environment and global health (Ferrauto and Heck, 1999; Williamson et al., 1985; Brandenberger et al., 2008), such as global warming, the destruction of the ozone layer, acid rain, and photochemical smog (He et al., 2002; Kryannikova et al., 2001). Three-way catalysts (TWCs) were used to control automotive emissions as early as 1977 in the US and Japan, since they can satisfy stringent standards and regulations (Nagai et al., 2008; Garin, 2004; Kašpar et al., 2003). Development efforts on TWCs to date has been extensive (Matsumoto, 2004; Martínez et al., 2001; Morikawa et al., 2008). As is well known, the platinum group metals (PM): Pt, Rh, and Pd, have been employed as the active components in TWCs, with an irreplaceable role due to their high activity and/or selectivity for many chemical reactions occurring in tailpipes (Gandhi et al., 2003; Shelef and McCabe, 2000). However, the improvement of TWCs currently centers on three key issues: (1) higher performance, (2) lower costs, and (3) higher NO*x* removal efficiency under lean conditions. The rapid increase in the number of cars and more stringent emission legislation create pressure for

* Corresponding author. E-mail: hehong@bjut.edu.cn

higher TWC performance. In addition, reduction of TWC cost is a crucial issue due to shortages of PM resources, prompting efforts to decrease PM loading requirements (Gaspar and Dieguez, 2000; Chen and Goodman, 2008). Therefore, high performance and low cost have become the driving force of TWC catalyst design and manufacture (Birgersson et al., 2006). TWC performance is determined by many synthetic factors, i.e. composition, chemical state (reduced and oxidized), metal dispersion, and active particle diameter. The ceria-zirconia solid solution (CZ) has been a key component in TWCs due to its beneficial role in improving stability and enhancing the water-gas shift reaction, as well as storing and releasing oxygen. But PM/CZ catalysts have showed low thermal stability as a result of the PM having low melting point and thermal stability. An important way for conventional TWCs to compensate for this deterioration has been to increase the amount of PM loading. In PM/CZ catalysts, the most frequent method of catalyst preparation is the wetness impregnation method, giving catalysts with less thermal stability, large particle size, small PM metallic surface area, and low metal dispersion (Kozlov et al., 2002; Morikawa et al., 2008; Adamopoulos and Papavasiliou, 2009; Li et al., 2007).

Much attention has been paid to the effects of preparation procedure on PM/CZ catalyst properties (Liu et al., 2009, 2010; Martínez-Arias et al., 2001; Fernández-García et al., 2004). Singh and Hegde (2010) prepared hierarchical $Ce_{1-x}M_xO_{2-y}$ (M = Pt or Pd, $0 < x < 0.1$) nanocrystallites by a sono-chemical method; these catalysts showed a high oxygen storage capacity, and Pt and Pd species on the catalyst surface have the high oxidation states of Pt^{4+} and Pd^{2+}. Papavasiliou et al. (2009) employed simultaneous co-precipitation, sequential co-precipitation, and wet impregnation to prepare Ce-Zr-La modified Pt/Al_2O_3 catalysts. The results showed that co-precipitation gave the catalysts with a superior structure, better thermal stability and higher activity as well as higher metal dispersion than conventional methods. Wang et al. (2011) had introduced the co-precipitation (supercritical drying and conventional drying), sol-gel, micro-emulsion, as well as impregnation methods to fabricate Pd/CZ-Al_2O_3 catalysts. The catalysts fabricated by co-precipitation (supercritical drying) and micro-emulsion exhibited relatively good textural properties and redox behavior as well as low T_{50} and T_{90}. Li et al. (2011) claimed that the supercritical drying process could improve catalysts reducibility and catalytic activity as well as oxygen storage capacity. Li et al. (2007) reported that the performance, phase structure, and adsorption abilities were significantly influenced by the preparation route.

Nanocatalysts have been attracted much attention because they exhibit excellent activity and selectivity for many chemical reactions (Qiao et al., 2011; Herzing et al., 2009; Wei et al., 2011). Qiao et al. (2011) synthesized the $Pt_1/FeOx$ catalysts, where the Pt species is anchored on the support surface with an isolated single Pt atom configuration, and the catalyst gave high activity for CO preferential oxidation in a hydrogen stream. Herzing et al. (2009) reported that the drying condition could significantly influence Au/Fe_2O_3 catalysts' performance. The Au showed a small cluster (< 0.5 nm) configuration over the catalyst Au/Fe_2O_3 dried in an air flow. Wei et al. (2011) employed a new method of gas bubbling-assisted membrane reduction to fabricate Au nanoparticles on three-dimensionally ordered macroporous $LaFeO_3$ and $Ce_{0.8}Zr_{0.2}O_2$ surfaces. The Au particles showed a small diameter of 2.8 nm on both $Au_{0.04}/LaFeO_3$ and $Au_{0.04}/Ce_{0.8}Zr_{0.2}O_2$ catalysts, which exhibited high activity for soot combustion with a low T_{10} of ca. 218–227°C and high CO_2 selectivity of 99.7%. Liu et al. (2009, 2010) reported that the Au-Rh/Al_2O_3 and $Pd/Ce_{0.5}Zr_{0.5}O_2$ catalysts fabricated by the ultrasonic-assisted membrane reduction (UAMR) method showed excellent activity and high dispersion of active particles with small diameter on the support.

However, the two processes of impregnation and *in-situ* reduction were used to fabricate nanocatalysts. These established the approaches to produce TWC catalysts with high activity, but failed to improve thermal stability or achieve cost reduction. Indeed, the above processes can significantly improve catalytic activity, but the catalysts' thermal stability and industrial applications will remain limited.

To solve these problems, the effects of preparation methods on 0.7 wt% Pt + 0.3 wt% $Rh/Ce_{0.6}Zr_{0.4}O_2$ catalyst performance were investigated. The results showed that the catalysts fabricated by UAMR-precipitation methods exhibited higher catalytic performance and better thermal stability as well as lower Pt-Rh loading with the same efficiency of pollutant removal. These catalysts were also characterized by XRD, TEM, N_2 adsorption, and hydrogen temperature programmed reduction (H_2-TPR) techniques.

To the best of our knowledge, this is the first time that the UAMR-precipitation approach has been used to fabricate a 0.7 wt% Pt + 0.3 wt% $Rh/Ce_{0.6}Zr_{0.4}O_2$ catalyst with high catalytic performance. In the pursuit of the optimal preparation method in catalyst design and development, this achievement can assist in synthesizing TWCs with high activity, good thermal stability, and low cost.

1 Experimental

All chemicals used in the experiments were of analytical grade and were purchased from the Sinopharm Group Chemical Reagent Co., and were used without further purification.

1.1 Pt and Rh nanoparticle colloid preparation

Pt and Rh nanoparticle colloids were fabricated by UAMR method developed in our laboratory (Liu et al., 2009,

2010). K_2PtCl_4 and $RhCl_3$ solutions were employed as the precursors and $NaBH_4$ was used as the reductant, and the UAMR reactor was placed in an ultrasonic bath at room temperature. In a typical process, the required amount of CTAB (cetyltrimethyl ammonium bromide) was dissolved in deionized water under vigorous stirring at 60°C in a water bath. Then the K_2PtCl_4 or $RhCl_3$ aqueous solution was added into the above solution with the$n_{[CTAB]}/n_{[Pt\ or\ Rh]}$ molar ratio of 50/1. The $NaBH_4$ solution stored in an ice bath was injected into the ceramic membrane reaction tubes (φ = 3 mm × 160 mm, Hyflux Group of Companies, Singapore) by a constantly flowing pump (HLB-2020, Satellite Factory, Beijing) with the flow rate of 1 mL/min, and the usage was determined by the $n_{[NaBH4]}/n_{[Pt\ or\ Rh]}$ ratio of 30/1. The mixed solution of Pt-CTAB or Rh-CTAB was driven by a peristaltic pump (Baoding Lange Co., Ltd., China) to cycle in the UAMR reactor, and the $NaBH_4$ solution was forced into the ceramic membrane tubes and infiltrated into the UAMR reactor through abundant holes ($d \approx 40$ nm) on the walls of the ceramic tubes. The Pt or Rh precursor was immediately reduced when the two solutions came in contact, and the color of the mixed solution changed from yellow to dark transparent black. The synthesis process was stopped when the reductant solution had been completely consumed, giving the Pt or Rh nanoparticle colloid that was reserved for use in the next step.

1.2 Catalyst preparation

Four types of 0.7 wt%Pt + 0.3 wt% $Rh/Ce_{0.6}Zr_{0.4}O_2$ catalysts were prepared by UAMR co-precipitation, UAMR separation precipitation, co-impregnation, and sequential impregnation methods.

In UAMR co-precipitation method, the calculated volume of Pt and Rh nanoparticle colloids were mixed together and then added to a mixed solution of $Ce(NO_3)_3{\cdot}6H_2O$ and $ZrO(NO_3)_2{\cdot}2H_2O$ under stirring. The pH of the obtained mixed solution was adjusted to the range of 10–11 by adding triethylamine (TEA) and the color of the solution changed from dark transparent black to brown-black. The yielded slurry was kept in an ultrasonic bath and stirred at 60°C for 0.5 hr, then filtered and washed with deionized water until no Cl^- ion could be detected. The obtained precipitate was dried at 80°C overnight and calcined at 550°C for 4.0 hr in a furnace, and the catalyst was denoted as Pt + Rh/CZ-A.

In the case of the UAMR separation precipitation process, the calculated volume of Pt nanoparticle colloid was first mixed with a $Ce(NO_3)_3{\cdot}6H_2O$ solution, and then the pH was adjusted to the range of 10–11. The Rh nanoparticle colloid was added to a $ZrO(NO_3)_3$ solution in a similar manner, then the two solutions were stirred at 60°C in an ultrasonic bath for 1 hr before being mixed together. The mixed slurry was further stirred at 60°C in an ultrasonic bath for 1 hr before being filtered, washed, dried and calcined under similar conditions as for the preparation of the Pt + Rh/CZ-A, and the obtained catalyst was denoted as Pt + Rh/CZ-B.

In the third method, co-impregnation, the $Ce_{0.6}Zr_{0.4}O_2$ support was prepared by a co-precipitation method. The desired mass of $Ce(NO_3)_3{\cdot}6H_2O$ and $ZrO(NO_3)_3$ with the ratio of Ce:Zr = 3:2 was dissolved together and TEA was employed as the precipitant to adjust the pH to 10–11. The yielded slurry was filtered, washed, dried, and calcined at 550°C for 4.0 hr in a furnace. The calculated amount of $Ce_{0.6}Zr_{0.4}O_2$ was impregnated with a mixed solution of K_2PtCl_4 and $RhCl_3$, and the as-prepared catalysts were dried at 80°C overnight and calcined at 550 °C for 4.0 hr, giving the catalyst denoted as Pt + Rh/CZ-C.

In the fourth method, sequential impregnation, the $Ce_{0.6}Zr_{0.4}O_2$ support was the same as for the Pt + Rh/CZ-C sample. The impregnation method was used to prepare the 0.7 wt% $Pt/Ce_{0.6}Zr_{0.4}O_2$ as-prepared catalyst and a dilute solution of K_2PtCl_4 was employed as the precursor. After the processes of drying (80°C) and calcination (550°C, 4.0 hr), the 0.7 wt% $Pt/Ce_{0.6}Zr_{0.4}O_2$ catalyst was impregnated in the $RhCl_3$ solution, giving the 0.7 wt%Pt + 0.3 wt% $Rh/Ce_{0.6}Zr_{0.4}O_2$ catalyst by repeating the above process, which was denoted as Pt + Rh/CZ-D.

In order to evaluate the hydrothermal stability of the catalysts, all samples were aged in a steam of 10% H_2O-90% air (*V/V*) at 900°C for 6.0 hr in a tube furnace.

1.3 Characterization

The specific surface areas and pore size distributions were investigated by N_2 adsorption at –196°C on a physical adsorption analyzer (ASAP 2020, Micromeritics). The samples were degassed at 250°C for 3.0 hr in a vacuum ($<1.33\times10^{-4}$ Pa) before being measured, and the results were automatically calculated by software supplied with the instrument.

The phase structure was investigated by an X-ray diffractometer (Rigaku D/Max-γ) operating at 45 kV and 35 mA with Cu $K\alpha$ radiation and graphite mono-chromator (λ = 1.5406 Å). The spectra were scanned from 20° to 80° at a rate of 0.02°/sec and the patterns recorded were referred to the powder diffraction files-1998 ICDD PDF database for phase identification. The intensities of the XRD peaks were calibrated using monocrystal silicon as a standard and the particle sizes of the catalysts were estimated using the Scherrer equation ($D = K\lambda/\beta\cos\theta$).

High resolution transmission electronic microscope (TEM) images were recorded on a JEM-2100 (JEOL, Ltd.) transmission electronic microscope with an accelerating voltage of 200 kV. The catalysts were reduced in a hydrogen stream (50 mL/min) at 300°C for 2.0 hr prior to the measurement, then ground, dispersed in isopropyl alcohol and deposited on a carbon film-coated copper grid.

The reducibility was measured by the H_2-TPR technique on a chemical adsorption analyzer (AutoChem 2920 II, Mi-

cromeritics) equipped with a TCD detector. In this process, a mass of 50 mg (40–60 mesh) catalyst was pretreated in a mixed flow of (50 mL/min) 20% O_2-80% N_2 (*V*/*V*) at 500°C for 1.0 hr in a U-type quartz tube micro reactor (i.d. = 4 mm). After being cooled to room temperature in the same atmosphere, the catalyst was purged by helium flow (50 mL/min) for 15 min, and then exposed to a mixed flow (50 mL/min) of 10% H_2-90% Ar (*V*/*V*) and heated from 30 to 850°C at a ramp rate of 10°C/min. The outlet gas was cooled by a mixture of isopropanol and liquid nitrogen to remove the water and monitored online by a TCD detector. The H_2 consumption was calibrated by CuO powder (Aldrich, 99.995%) as a reference.

The metal dispersion was investigated by CO pulse chemisorption on the analyzer as used in the H_2-TPR measurement. The sample (50 mg, 40–60 mesh) was first pretreated in a mixed flow of (50 mL/min) 10% H_2-90% Ar (*V*/*V*) at 300°C for 0.5 hr and purged by the Ar flow (50 mL/min) for 0.5 hr at 350°C. After being cooled to room temperature with the same atmosphere, CO was pulsed into the reactor. The CO signal was detected online by a TCD detector.

1.4 Catalytic activity evaluation

The catalytic activities for the TWC reactions were evaluated in a continuous flow fixed-bed micro quartz tube reactor (i.d. = 8 mm) at atmospheric pressure. A mass of 0.5 g (1.0 mL) catalyst (40–60 mesh) was mixed with 3.0 g quartz sand (40–60 mesh) to diminish the effect of the reaction heat. The sample was fixed in the middle of a micro quartz tube reactor between two quartz wool plugs, and the reactor was placed in a furnace equipped with a programmable temperature controller. The volumetric composition of the reaction stream (1000 mL/min) was 1.6%CO + 0.05% HC + 0.1% NO*x* + 1.0% O_2 + 0.23% H_2, balanced by N_2 with the corresponding space velocity of 60000 hr^{-1}. The concentrations of CO, HC, and NO*x* in the effluent were monitored on-line by a five-component automotive emission analyzer (MEXA-584L, HORIBA). The λ (air/fuel) was calculated and regulated according to the formula of $(2[O_2]+[NO])/([H_2]+[CO]+10[C_3H_8]+9[C_3H_6])$ (Wang et al., 2011; Nagai et al., 2006). The λ value was as adjusted to 0.8, 0.88, 0.92, 1.0, 1.08, 1.12, 1.15, and 1.20 by changing the oxygen concentration in the reaction gas. The operation window limit, i.e. λ window, for three-way catalytic reactions was defined as the ratio of air/fuel for the 80% conversion of CO, HC, and NO*x* at a given temperature.

2 Results and discussion

2.1 Catalytic performance

The catalytic activities for three-way reactions over the Pt + Rh/CZ catalysts are presented in **Fig. 1**.

It can be seen that the catalysts prepared from the Pt

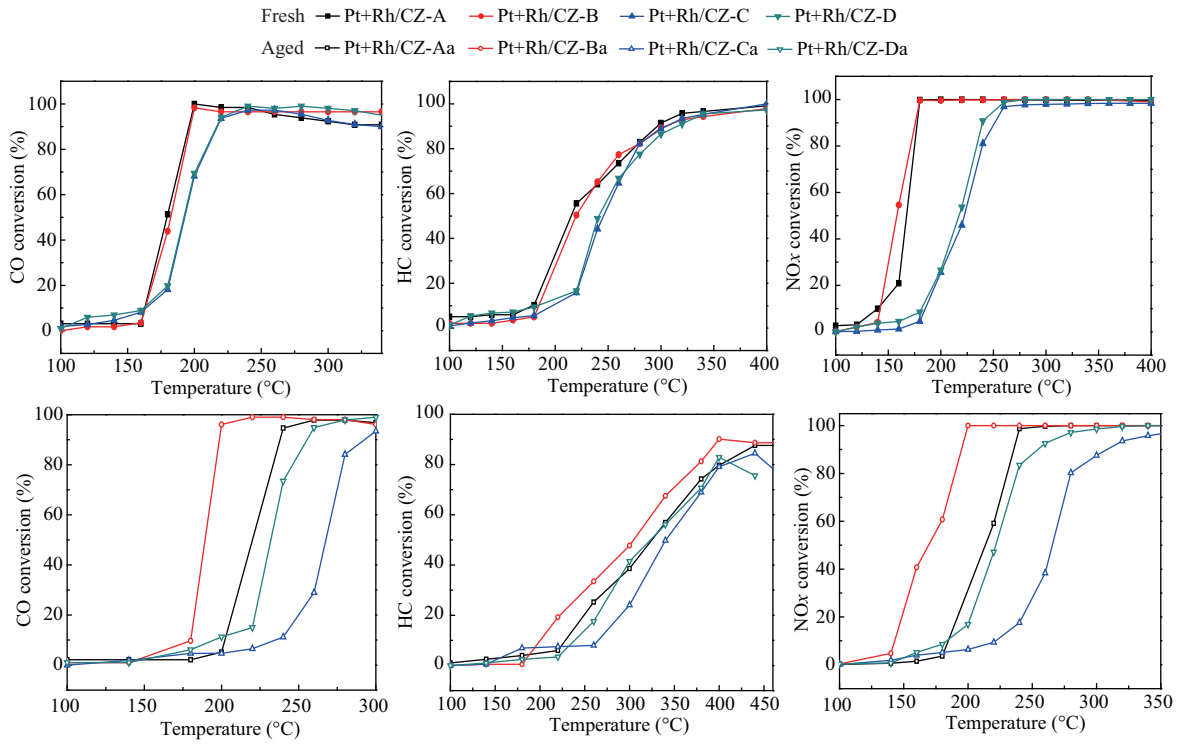

Fig. 1 Conversion of CO, HC, and NO*x* over fresh and aged Pt + Rh/CZ-A, B, C, or D for the three-way catalytic reaction. Reaction condition: 1.6% CO+1.0% O_2 +0.05% HC (C_3H_8+C_3H_6)+0.1% NO*x*, N_2 balance; space velocity = 60,000 hr^{-1}.

and Rh nanoparticles exhibited relatively better catalytic activity than the corresponding impregnation samples. However, in fresh catalysts, no significant difference in activity could be observed over the former two catalysts (Pt + Rh/CZ-A and Pt + Rh/CZ-B) and a similar situation was also found with the latter two catalysts (Pt + Rh/CZ-C and Pt + Rh/CZ-D).

As for the aged catalysts, the activities for three-way reactions increased in the order of Pt + Rh/CZ-Da < Pt + Rh/CZ-Ca < Pt + Rh/CZ-Aa < Pt + Rh/CZ-Ba. The results revealed that the three-way catalysts showed high activity when the Pt and Rh nanoparticles were employed as the precursor, and the preparation method was another key factor affecting catalyst performance. In order to compare performance, the light-off (T_{50}, defined as the temperature where CO, HC, and NOx obtained 50% conversion), full conversion (T_{90}, defined as the temperature where CO, HC, and NOx obtained 90% conversion) temperatures and the ΔT(defined as $T_{90} - T_{50}$) for all catalysts are summarized in **Table 1**.

It can be seen that the catalysts prepared from nanoparticles (Pt + Rh/CZ-A and Pt + Rh/CZ-B) exhibited relatively lower T_{50} and T_{90} values than the catalysts fabricated by the impregnation method. The T_{50} for the CO oxidation were 180, 182, 193, and 194°C, and 215, 219, 246, and 241°C for HC oxidation were obtained over the fresh Pt + Rh/CZ-A, Pt + Rh/CZ-B, Pt + Rh/CZ-C and Pt + Rh/CZ-D catalysts, respectively. In the case of NOx reduction, the T_{50} over the above catalysts was 167, 157, 223 and 217°C, respectively. As for the aged samples, the catalyst Pt + Rh/CZ-Ba exhibited the lowest T_{50} and T_{90} for the three-way catalytic reactions.

ΔT is another parameter to determine the three-way catalytic performance. It can be seen from **Table 1** that the ΔT for CO and HC oxidations was 15, 15, 24, and 24°C as well as 81, 86, 59, 69°C over Pt + Rh/CZ-A, Pt + Rh/CZ-B, Pt + Rh/CZ-C and Pt + Rh/CZ-D with the corresponding ΔT of 11, 17, 29, and 23°C for NOx reduction, respectively. As for the Pt + Rh/CZ-Ba catalyst that possessed the best activities, the T_{50} for CO and HC oxidation as well as the NOx reduction were 189, 305, and 169°C, respectively. Air/fuel ratio (λ) is a crucial factor to determine catalytic performance. Therefore, the function of λ and activities was investigated at 400°C, and the results are summarized in **Fig. 2**.

It can be seen that the conversion of CO and HC

Table 1 The light-off (T_{50}) and full conversion (T_{90}) temperature for three way catalytic reactions over 0.7 wt% Pt + 0.3 wt % $Rh/Ce_{0.6}Zr_{0.4}O_2$ catalysts

Samples	CO (°C)			HC (°C)			NO (°C)		
	T_{50}	T_{90}	ΔT	T_{50}	T_{90}	ΔT	T_{50}	T_{90}	ΔT
Pt + Rh/CZ-A	180	195	15	215	296	81	167	178	11
Pt + Rh/CZ-B	182	197	15	219	305	86	157	174	17
Pt + Rh/CZ-C	193	217	24	246	305	59	223	252	29
Pt + Rh/CZ-D	194	218	24	241	310	69	217	240	23
Pt + Rh/CZ-Aa	220	238	18	326	/	/	213	236	23
Pt + Rh/CZ-Ba	189	199	10	305	398	93	169	195	26
Pt + Rh/CZ-Ca	267	292	25	341	/	/	265	309	44
Pt + Rh/CZ-Da	232	255	23	306	/	/	222	254	32

T_{50} and T_{90} are defined as the temperature when CO, HC, and NOx obtained 50% and 90% conversion, ΔT is defined as $T_{90} - T_{50}$.

/: denotes that the full conversion was not obtained at the tested temperature.

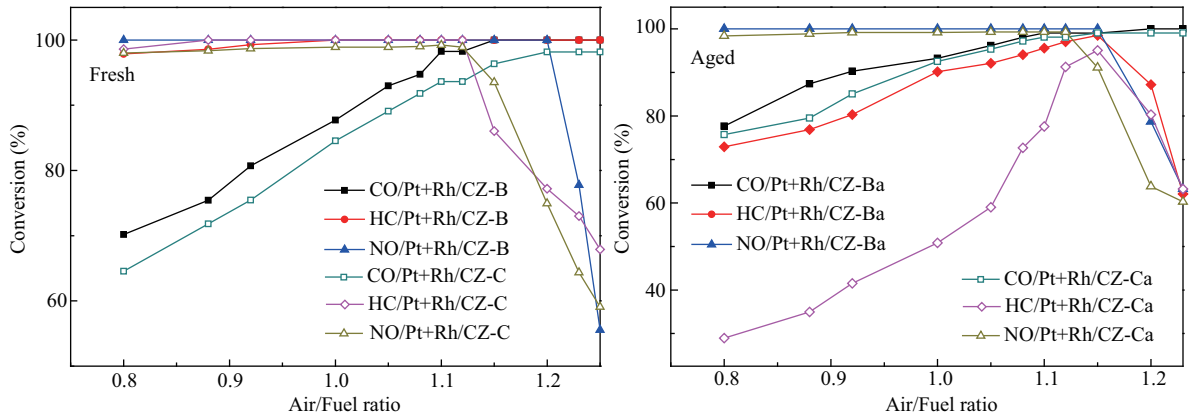

Fig. 2 CO, HC, and NO conversion over fresh and aged Pt + Rh/CZ-B and Pt + Rh/CZ-C catalysts at different air/fuel ratios.

oxidation increased with elevated λ and reached ca. 90% at λ = 1.1, and the NO conversion was ca. 100% at λ < 1.15 over the fresh and aged Pt + Rh/CZ-B and Pt + Rh/CZ-C catalysts. The levels of CO oxidation and NO reduction over fresh Pt + Rh/CZ-B were higher than those over the Pt + Rh/CZ-C catalyst. As for the HC oxidation, the Pt + Rh/CZ-B catalyst showed much higher conversion in the λ range from 1.15 to 1.23 than that of the Pt + Rh/CZ-C sample. In the case of the aged sample, no significant changes could be found for CO oxidation and NO reduction. However, an obvious decrease for HC oxidation could be observed in the λ range from 0.8 to 1.15 over Pt + Rh/CZ-Ca. Therefore, the catalyst Pt + Rh/CZ-B exhibited relatively higher activities and thermal stability than Pt + Rh/CZ-C.

The working window is important for TWCs to meet the stringent emission regulations. The working windows for all catalysts were calculated from the activity curves and the results are shown in **Table 2**. The working window is defined as $\Delta\lambda = \lambda_{max} - \lambda_{min}$, where λ_{max} is defined as the λ at 80% of NO*x* conversion under lean conditions and the λ_{min} as the λ at 80% CO or C_3H_8 conversion under rich conditions.

It can be seen that the Δλ was 0.425, 0.427, 0.386, and 0.384 over Pt + Rh/CZ-A, Pt + Rh/CZ-B, Pt + Rh/CZ-C, and Pt + Rh/CZ-D catalysts, respectively. In the case of aged samples, the Δλ decreased to 0.284, 0.287, 0.065, and 0.115 correspondingly. It was not surprising that the Pt + Rh/CZ-B catalyst had the largest λ operation window for the three-way catalytic reactions.

2.2 Specific surface area, Pore size, and Crystal structure

Figure 3 shows the isotherms and pore distribution of fresh catalysts. All samples showed a typical IV type isotherm with a pronounced H3-type hysteresis loop, which clearly indicated that the samples had a mesoporous structure with the pores interlaced together. The different relative pressures of the hysteresis loops indicated the discrepancy in pore size distributions. The specific surface areas of Pt + Rh/CZ-A and Pt + Rh/CZ-B catalysts were 60.2 and 67.6 m^2/g, respectively, which was higher than those of the Pt + Rh/CZ-C (29.1 m^2/g) and Pt + Rh/CZ-D (29.0 m^2/g) samples. The pore volume varied in the sequence of Pt + Rh/CZ-B (0.15 cm^3/g) > Pt + Rh/CZ-A (0.14 cm^3/g) > Pt + Rh/CZ-D (0.11 cm^3/g) > Pt + Rh/CZ-C (0.10 cm^3/g). In the case of aged samples, the specific surface area and pore volume decreased significantly for all tested samples, and the specific surface areas of Pt + Rh/CZ-Aa (21.2 m^2/g) and Pt + Rh/CZ-Ba (18.5 m^2/g) were higher than those of Pt + Rh/CZ-Ca (8.5 m^2/g) and Pt + Rh/CZ-Da (8.1 m^2/g). The pore volumes of Pt + Rh/CZ-Aa and Pt + Rh/CZ-Ba were about ten times larger than those of Pt + Rh/CZ-Ca and Pt + Rh/CZ-Da.

Table 2 Air/fuel ratio (λ) windows of 0.7 wt% Pt + 0.3 wt % $Rh/Ce_{0.6}Zr_{0.4}O_2$ catalysts

Sample	λ^a_{min}	λ^b_{max}	$\Delta\lambda = \lambda_{max} - \lambda^c_{min}$
Pt + Rh/CZ-A	0.800[c]	1.225	0.425
Pt + Rh/CZ-B	0.800[c]	1.227	0.427
Pt + Rh/CZ-C	0.800[c]	1.186	0.386
Pt + Rh/CZ-D	0.800[c]	1.184	0.384
Pt + Rh/CZ-Aa	0.896	1.180	0.284
Pt + Rh/CZ-Ba	0.919	1.197	0.287
Pt + Rh/CZ-Ca	1.104	1.169	0.065
Pt + Rh/CZ-Da	1.063	1.178	0.115

[a] λ_{min} is defined at 80% of CO or C_3H_8 conversion, [b] λ_{max} is defined at 80% of the NO conversion, [c] the value was the lowest λ in experiment, the λ value was adopted in the range of λ = 0.8–1.23

With the UAMR-precipitation methods, the Pt and Rh nanoparticle surfaces were covered by several layers of CTAB molecules. Under basic conditions, the Ce and Zr species could incorporate into the CTAB chains and agglomerate around the Pt and Rh particles to form core-shell-like polymeric structures. The CTAB played the dual function of stabilization of the Pt and Rh particles and enhancement of the formation of the porous structure within the catalysts. The hysteresis loop in the N_2 absorption-desorption curve closed at relatively lower P/P_0 in the region of low pressure, suggesting that the catalyst consisted of an appropriate ratio of micro- and mesopores, with an abundance of micro-porous structures.

The XRD patterns of fresh and aged catalysts are shown in **Fig. 4**. It can be seen that the diffraction peaks for all catalysts could be well indexed in the 2θ range of 20–80° with a face-centered cubic fluorite structure (JCPDS No. 38-1439). The crystallite sizes of the fresh catalysts were 11.2, 12.8, 15.0, and 16 nm for Pt + Rh/CZ-A, Pt + Rh/CZ-B, Pt + Rh/CZ-C, and Pt + Rh/CZ-D, respectively. No other peaks of Pt and/or Rh species or impurities could be observed, which was due to the Pt and Rh species having low concentration or being highly dispersed on the catalyst surface. The phase separation of tetragonal ZrO_2 could be observed in the XRD patterns of the Pt + Rh/CZ-C and Pt + Rh/CZ-D catalysts.

For the aged samples, the intensities of the diffraction peaks increased and narrowed, indicating that the catalysts were sintered and the particles became larger than those of fresh ones. The phase separation of tetragonal ZrO_2 could be observed for all aged samples, showing the monoclinic phase in Pt + Rh/CZ-Aa and Pt + Rh/CZ-Ba, and tetragonal ZrO_2 in Pt + Rh/CZ-Ca and Pt + Rh/CZ-Da samples. Furthermore, Pt diffraction peaks were observed for the Pt + Rh/CZ-Ca and Pt + Rh/CZ-Da samples at 39.8° and 46.4° due to Pt species being significantly sintered, indicating that the catalysts prepared by the impregnation method showed low thermal stability. However, Pt species remained highly dispersed over the

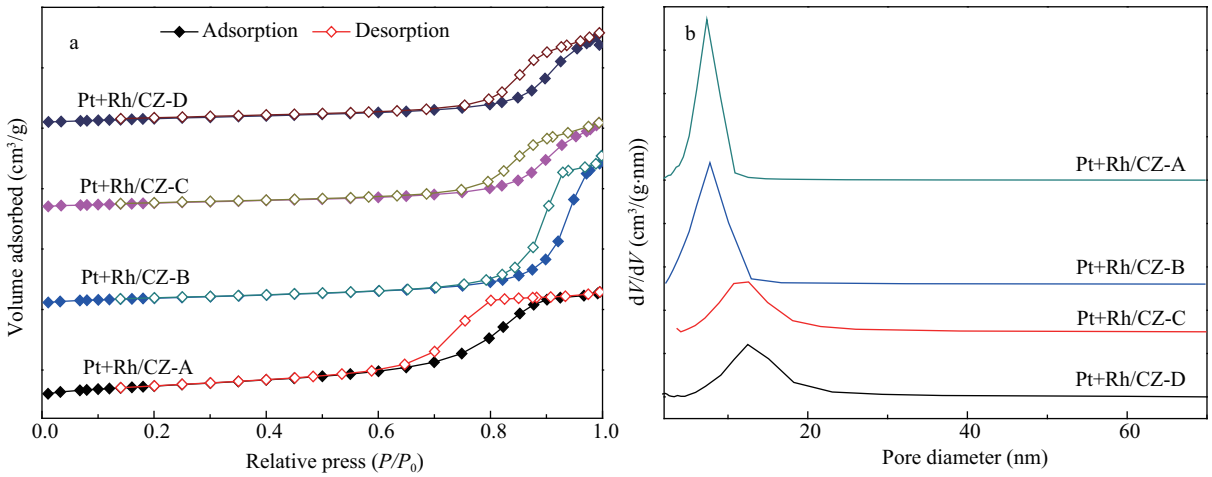

Fig. 3 N_2 adsorption–desorption isotherms (a) and BJH pore size distribution (b) of fresh Pt + Rh/CZ-A, Pt + Rh/CZ-B, Pt + Rh/CZ-C, and Pt + Rh/CZ-D catalysts.

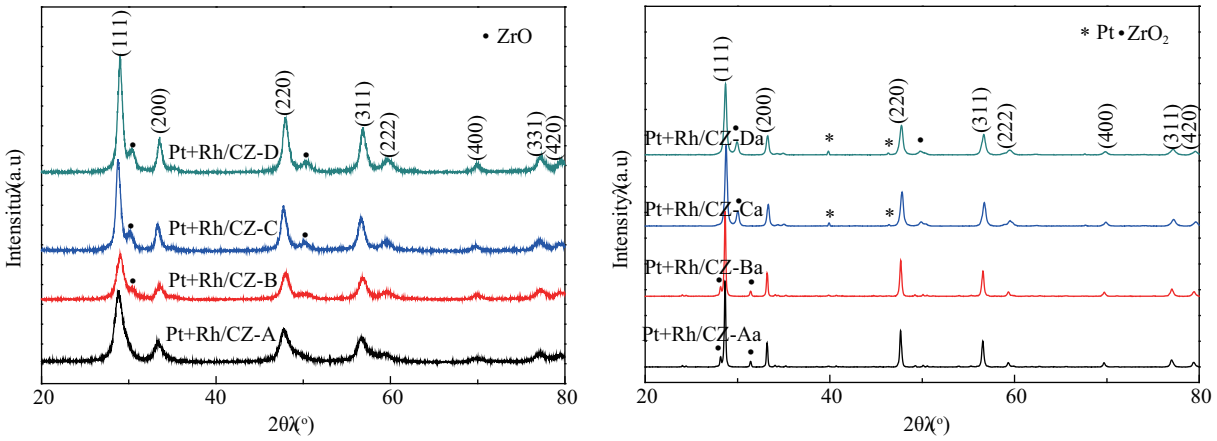

Fig. 4 The XRD profiles of fresh and aged Pt + Rh/CZ-A, Pt + Rh/CZ-B, Pt + Rh/CZ-C, and Pt + Rh/CZ-D catalysts.

CZ surface in the catalysts of Pt + Rh/CZ-Aa and Pt + Rh/CZ-Ba. In the preparation process, Ce and Zr species were incorporated into the CTAB molecules and around the Pt and Rh nanoparticles, thus, the thermal stability of the metal nanoparticles increased and the interaction between Ce, Zr ions and metal particles was enhanced (Luo et al., 2009).

The metal dispersions of all catalysts were measured and presented in **Table 3**. It can be seen that the metal dispersion (Pt + Rh) of Pt + Rh/CZ-A (35.7%) and Pt + Rh/CZ-B (43.2%) was lower than that of Pt + Rh/CZ-C (51.6%) and Pt + Rh/CZ-D (52.2%), with active particle diameters of 2.6, 2.6, 2.2, and 2.2 nm, respectively. The metallic surface area (Pt + Rh) of the catalysts decreased in the order Pt + Rh/CZ-D (159.0 m^2/g) > Pt + Rh/CZ-C (157.1 m^2/g) > Pt + Rh/CZ-B (131.8 m^2/g) > Pt + Rh/CZ-A (105.4 m^2/g). As for the aged catalysts, the metal dispersion was 32.2%, 42.2%, 12.4%, and 14.7% over the Pt + Rh/CZ-Aa, Pt + Rh/CZ-Ba, Pt + Rh/CZ-Ca, Pt + Rh/CZ-Da samples, with the metallic surface areas of 99.8, 130.2, 37.9 and 44.7 m^2/g, respectively. No significant changes could be observed in the metal dispersion of the former two catalysts after aging. However, the metal dispersion of the Pt + Rh/CZ-Ca and Pt + Rh/CZ-Da samples decreased significantly, suggesting that the metal species of the former two catalysts were more stable. So, it is reasonable for the Pt + Rh/CZ-Aa, Pt + Rh/CZ-Ba catalysts to have good catalytic performance.

In the UAMR-precipitation method, the nanoparticles of Pt and/or Rh were protected by CTAB, thus, every metal particle was capped by many CTAB molecules to form the polymeric structure O-$NC_{19}H_{42}$-($Pt_{1/n}$ and/or $Rh_{1/n}$). The metal ions Ce^{4+} and/or Zr^{4+} were precipitated to form $M(H_2O)_x(OH)_y^{(4-y)+}$ (M = Ce, Zr) structures, which could incorporate into the CTAB chains in the basic condition and presence of nanoparticles. A high net negative charge aggregated on these $M(H_2O)_x(OH)_y^{(4-y)+}$ surfaces and a gelatinous hydrous hydroxide was obtained under the highly basic conditions (pH: 10–11). In order to reduce the net negative charge, the proton abstraction reaction was deduced to neutralize the surface net charges and form the oxo-bridge (MOH-O-HOM) (Parks, 1965).

Table 3 Physico-chemical properties of 0.7 wt% Pt + 0.3 wt % $Rh/Ce_{0.6}Zr_{0.4}O_2$ catalysts

Sample	Surface area (m^2/g)	Pore volume (cm^3/g)	Pore size (nm)	Metal dispersion (%)	Metallic surface area		Active particle diameter (nm)	Crystal size[c] (nm)
					Sample (m^2/g)	metal (m^2/g)		
Pt + Rh/CZ-A	60.2	0.144	8.4	48.4[a]/35.7[b]	1.2[a]/1.1[b]	117.5[a]/105.4[b]	2.6[a]/2.6[b]	11.2
Pt + Rh/CZ-B	67.6	0.148	10.5	54.9/43.2	1.4/1.3	135.5/131.8	2.1/2.6	12.8
Pt + Rh/CZ-C	29.1	0.104	14.9	65.4/51.6	1.6/1.6	161.5/157.1	1.7/2.2	15.0
Pt + Rh/CZ-D	29.0	0.109	14.8	66.2/52.2	1.6/1.6	163.4/159.0	1.7/2.2	16.0
Pt + Rh/CZ-Aa	21.2	0.049	28.8	41.5/32.2	1.0/1.0	102.5/99.8	2.7/3.5	28.5
Pt + Rh/CZ-Ba	18.5	0.040	29.2	51.2/42.2	1.3/1.3	133.8/130.2	2.1/2.7	29.3
Pt + Rh/CZ-Ca	8.5	0.005	30.1	15.8/12.4	0.4/0.4	38.9/37.9	7.2/9.1	29.8
Pt + Rh/CZ-Da	8.1	0.005	29.6	18.6/14.7	0.5/0.5	45.9/44.7	6.1/7.7	27.7

[a] Calculated based on Pt; [b] calculated based on Pt + Rh; [c] the crystal size of the samples was calculated on an XRD peak from the (111) plane using a Scherrer equation.

Abundant MOH-O-HOM interacted with the Pt and/or Rh particles to form a polymeric hydrous oxide (nMO_x(O-CTAB-$Pt_{1/n}$ and/or $Rh_{1/n})_y mH_2O$) and the Pt and/or Rh particles were stabilized in the center of the polymeric hydrous hydroxides to improve the metal dispersion (Terribile et al., 1998). In the TWC catalysts, the chemical states of the active particles had significant influence on the performance. In the Pt + Rh/CZ-A and Pt + Rh/CZ-B catalysts, Pt and Rh nanoparticles were employed as the precursors, and part of the Pt and Rh atoms on the particle surfaces were oxidized to give PtO*x* and RhO*x* species with high activity. The Rh species could have a lower oxygen coordination number when Rh was loaded on ZrO_2 (Nagai et al., 2008; Shinjoh et al., 2009). The result was that the Rh had a metallic or relatively low oxidation state, resulting in strong potential for the NO*x* reduction reaction. These hypotheses should be verified by more detailed investigation in further studies.

TEM images of the catalysts are shown in **Fig. 5**. No Pt or Rh species could be found on the TEM images, which may be due to the high dispersion of the Pt and Rh species. It can be seen that the particle sizes of Pt

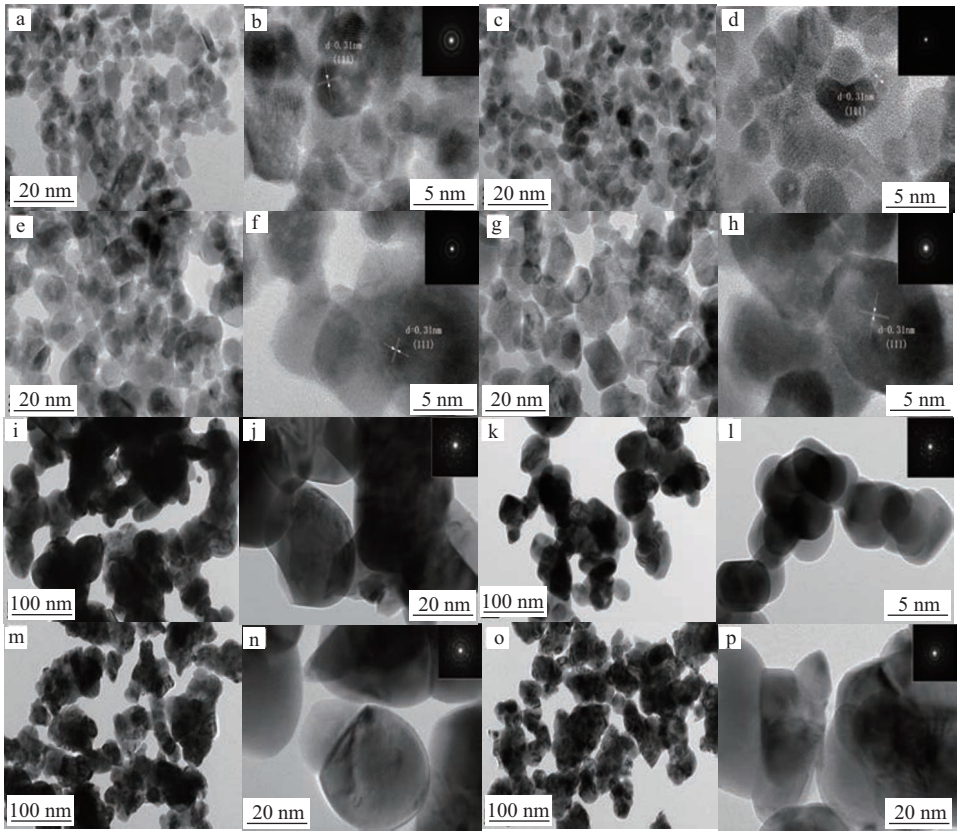

Fig. 5 TEM, high-resolution images and SAED patterns (insets) of fresh and aged. (a, b) Pt + Rh/CZ-A; (c, d) Pt + Rh/CZ-B; (e, f) Pt + Rh/CZ-C; (g, h) Pt + Rh/CZ-D; (i, j) Pt + Rh/CZ-Aa; (k, l) Pt + Rh/CZ-Ba; (m, n) Pt + Rh/CZ-Ca; and (o, p) Pt + Rh/CZ-Da.

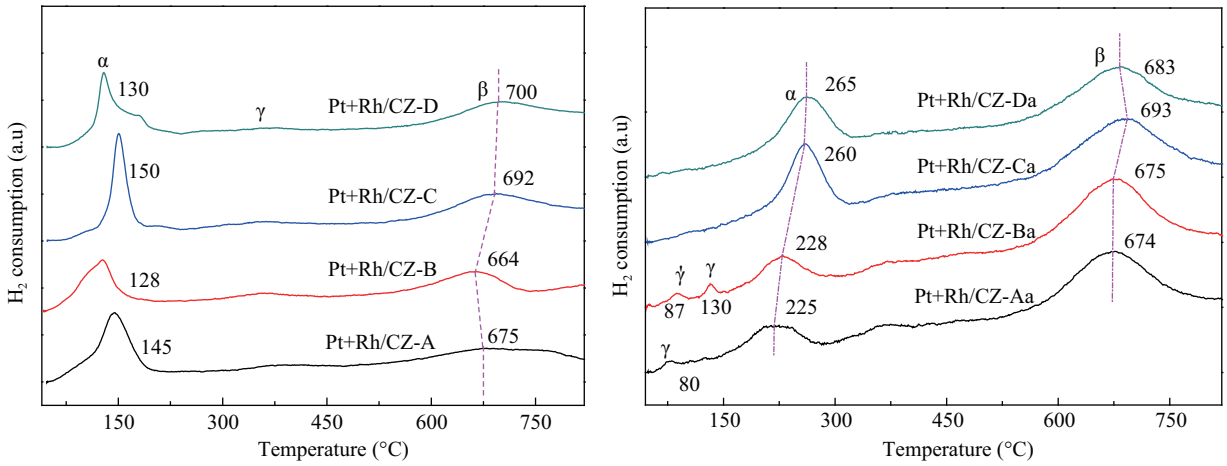

Fig. 6 H_2-TPR profiles of fresh and aged Pt + Rh/CZ-A, Pt + Rh/CZ-B, Pt + Rh/CZ-C, and Pt + Rh/CZ-D catalysts.

+ Rh/CZ-A and Pt + Rh/CZ-B were smaller than those of the Pt + Rh/CZ-C and Pt + Rh/CZ-D catalysts. The lattice fringes with distance of 0.31 nm could be assigned to the (111) crystal plane of $Ce_{0.6}Zr_{0.4}O_2$(JCPDS No. 38-1439), and this suggested that the $Ce_{0.6}Zr_{0.4}O_2$ crystallites showed preferential exposure of the (111) plane. For the aged catalysts, the particle size obviously increased, while the Pt + Rh/CZ-A and Pt + Rh/CZ-B particle sizes were still smaller than those of Pt + Rh/CZ-C and Pt + Rh/CZ-D. Therefore, the results again revealed that the UAMR-preparation method was beneficial for improving the thermal stability of the catalysts, which agreed well with the N_2 adsorption results.

2.3 H_2-TPR measurement

Figure 6 shows the H_2-TPR profiles of all catalysts. Only two reduction peaks were observed on fresh catalysts; the first one could be assigned to the reduction of the PtO*x* and RhO*x* species, as well as surface or subsurface Ce^{4+} species, at a temperature range of 120–150°C (Wang et al., 2011; Conner and Falconer, 1995; Bera et al., 2003; Dutta et al., 2007). The second peak at 670–700°C could be ascribed to the reduction of the lattice oxygen of $Ce_{0.6}Zr_{0.4}O_2$ (Morikawa et al., 2008; Nishihata et al., 2002). The H_2 consumption at low temperature (120–150°C) was 0.28, 0.27, 0.32, and 0.30 mm/g catalyst over the Pt + Rh/CZ-A, Pt + Rh/CZ-B, Pt + Rh/CZ-C, and Pt + Rh/CZ-D catalysts, and the second peaks were at 675, 664, 692, and 700°C with the H_2 consumption of 0.17, 0.18, 0.26, and 0.24 mm/g catalyst over the above catalysts, respectively. Attention should be paid to the fact that the Pt + Rh/CZ-B catalyst has the lowest reduction temperature and the corresponding aged sample gave a similar result, indicating that the Pt and Rh species on the Pt + Rh/CZ-B catalyst possessed better reducibility. Based on H_2 consumption, the Pt and Rh species exhibited a lower oxidative state for the catalyst fabricated from the UAMR precipitation method. We can conclude that preparation route can significantly influence the PM chemical state (Papavasiliou and Shinjoh, 2009; Nagai et al., 2006).

As for the aged catalysts, the first reduction peaks shifted to high temperature, whereas the temperature of the second peaks remained almost unchanged. It should be noted that a new peak at ca. 80°C (Pt + Rh/CZ-Aa) and two reduction peaks at 87 and 130°C (Pt + Rh/CZ-Ba) could be observed. The additional peaks may due to the reduction of the highly dispersed PtO*x* and/or RhO*x* species. The H_2 consumption of the first reduction peak was 0.06, 0.05, 0.17, and 0.14 mm/g catalyst for Pt + Rh/CZ-Aa, Pt + Rh/CZ-Ba, Pt + Rh/CZ-Ca, and Pt + Rh/CZ-Da, respectively. As is known, the Pt and Rh species in the former catalysts were prepared from nanoparticles with zero valence. It was suspected that only part of the Pt and Rh atoms on the nanoparticle surface were oxidized into PtO*x* and/or RhO*x* species, which might be expected to form as Pt@PtO*x* and/or Rh@RhO*x* nanoparticles during the calcination and aging process. Therefore, it was reasonable that the former two samples had relatively low H_2 consumption. It can be concluded that the UAMR-precipitation method is a good way to produce three-way catalysts.

3 Conclusions

Four types of 0.7 wt% Pt + 0.3 wt% Rh/$Ce_{0.6}Zr_{0.4}O_2$ catalysts were prepared by different methods. The results showed that samples prepared by UAMR precipitation exhibited higher activity and thermal stability as well as better low temperature reducibility, and had specific surface areas of 60–67 and 18–22 m^2/g over the fresh and aged samples, respectively, whereas the specific surface area of the aged conventional catalyst was ca. 8 m^2/g. Moreover, the UAMR-precipitation-prepared samples exhibited better anti-sintering performance, and the aged catalysts showed high metal dispersion (41%–55%) and small particle diameter (2.1–2.7 nm), compared to 14%–

19% (metal dispersion) and 6.1–7.2 nm (particle diameter) for the aged samples prepared by impregnations.

In aged samples, the catalysts prepared by UAMR precipitation exhibited a wider λ window of 0.284–0.287, which was wider than that of conventional ones, having a λ window of 0.065–0.115. The catalysts prepared by UAMR precipitation were far superior to the conventional ones in terms of activity and thermal stability. The catalyst fabricated by UAMR separation precipitation showed the highest catalytic activities, and the T_{50} and T_{90} values for NO reduction were ca. 169 and 195°C, which were lower than those of the conventional catalysts of 265 and 309°C, respectively.

Finally, it can be concluded that the preparation procedure is a pivotal factor to affect the catalyst performance and thermal stability. The catalysts prepared by UAMR-precipitation methods exhibited excellent catalytic performance and thermal stability. Thus, the UAMR-separation precipitation method is an ideal approach to fabricate catalysts having excellent activity, thermal stability, high metal dispersion, and large specific surface area.

Acknowledgments

This work was supported by the National Nature Foundation of China (No. 21277009), the Beijing National Nature Foundation (No. 2101002), the Funding Project for Academic Human Resources Development in Institutions of Higher Learning under the Jurisdiction of Beijing Municipality (No. PHR201107104, PHR200907105), the National Research and Development Program (863) of China (No. 2011AA03A406), and the National Industrial Project of New Rare Earth Materials.

REFERENCES

Adamopoulos, O., Björkman, E., Zhang, Y., Muhammed, M., Bog, T., Mussmann, L. et al., 2009. A nanophase oxygen storage material: alumina-coated metal-based ceria. J. Europ. Ceram. Soc. 29(4), 677–689.

Bera, P., Priolkar, K. R., Gayen, A., Sarode, P. R., Hegde, M. S., Emura, S. et al., 2003. Ionic dispersion of Pt over CeO_2 by the combustion method: Structural investigation by XRD, TEM, XPS, and EXAFS. Chem. Mater. 15(10), 2049–2060.

Birgersson, H., Boutonnet, M., Klingstedt, F., Murzin, D. Y., Stefanov, P., Naydenov, A., 2006. An investigation of a new regeneration method of commercial aged three-way catalysts. Appl. Catal. B 65(1-2), 93–100.

Brandenberger, S., Kröcher, O., Tissler, A., Althoff, R., 2008. The state of the art in selective catalytic reduction of NO*x* by ammonia using metal-exchanged zeolite catalysts. Catal. Rev. 50(4), 492–531.

Chen, M. S., Goodman, D. W., 2008. Catalytically active gold on ordered titania supports. Chem. Soc. Rev., 37(9), 1860–1870.

Conner, W. C., Falconer, J. L., 1995. Spillover in heterogeneous catalysis. Chem. Rev. 95(3), 759–788.

Dutta, G., Waghmare, U. V., Baidya, T., Hegde, M. S., 2007. Hydrogen spillover on CeO_2/Pt: Enhanced storage of active hydrogen. Chem. Mater. 19(26), 6430–6436.

Fernández-García, M., Iglesias-Juez, A., Martínez-Arias, A., Hungría, A. B., Anderson, J. A., Conesa, J. C. et al., 2004. Role of the state of the metal component on the light-off performance of Pd-based three-way catalysts. J. Catal. 221(2), 594–600.

Fernández-García, M., Martínez-Arias, A., Iglesias-Juez, A., Hungría, A. B., Anderson, J. A., Conesa, J. C. et al., 2001. New Pd/CexZr1-$x$$O_2$/$Al_2O_3$ three-way catalysts prepared by microemulsion Part 1. Characterization and catalytic behavior for CO oxidation. Appl. Catal. B 31(1), 39–50.

Ferrauto, R. J., Heck, R. M., 1999. Catalytic converters: State of the art and perspectives. Catal. Today 51(3-4), 351–360.

Gandhi, H. S., Graham, G. W., McCabe, R. W., 2003. Automotive exhaust catalysis. J. Catal. 216, 433–442.

Garin, F., 2004. Environmental catalysis. Catal. Today 89(3), 255–268.

Gaspar, A. B., Dieguez, L. C., 2000. Dispersion stability and methylcyclopentane hydrogenolysis in Pd/Al_2O_3 Catalysts. Appl. Catal. A 201(2), 241–251.

He, H., Dai, H. X., Ng, L. H., Wong, K. W., Au, C. T., 2002. Pd-, Pt-, and Rh-Loaded Ce0.6Zr0.35Y0.05O_2 three-way catalysts: An investigation on performance and redox properties. J. Catal. 206(1), 1–13.

Herzing, A. A., Kiely, C. J., Carley, A. F., Landon, P., Hutchings, G. J., 2009. Identification of active gold nanoclusters on iron oxide supports for CO oxidation. Science 321(5894), 1331–1335.

Kašpar, J., Fornasiero, P., Hickey, N., 2003. Automotive catalytic converters: Current status and some perspectives. Catal. Today 77(4), 419–449.

Kozlov, A. I., Kim, D. H., Yezerets, A., Andersen, P., Kung, H. H., Kung, M. C., 2002. Effect of preparation method and redox treatment on the reducibility and structure of supported ceria-zirconia mixed oxide. J. Catal. 209(2), 417–426.

Kryannikova, L. N., Aksenov, A. A., Markaryan, G. L., Muravéva, G. P., Kostyuk, B. G., Kharlanov, A. N. et al., 2001. The redox treatments influence on the structure and properties of M_2O_3-CeO_2-ZrO_2 (M=Y, La) solid solutions. Appl. Catal. 210, 225–235.

Li, G. F., Wang, Q. Y., Zhao, B., Zhou, R. X., 2011. Promoting effect of synthesis method on the property of nickel oxide doped CeO_2-ZrO_2 and the catalytic behavior of Pd-only three-way catalyst. Appl. Catal. B 105(1-2), 151–162.

Li, J. H., Li, W, Kang, S. F., Ke, R., 2007. Comparison of NO adsorbing ability and process on Pt/Mg/Al oxide catalysts prepared by different methods. Catal. Lett. 116(3-4), 155–160.

Liu, L. C., Guan, X., Li, Z. M., Zi, X. H., Dai, H. X., He, H., 2009. Supported bimetallic AuRh/γ-Al_2O_3 nanocatalyst for the selective catalytic reduction of NO by propylene. Appl. Catal. B. 90, 1–9.

Liu, L. C., Wei, T., Zi, X. H., He, H., Dai, H. X., 2010. Research on assembly of nano-Pd colloid and fabrication of supported Pd catalysts from the metal colloid. Catal. Today 153(3-4), 162–169.

Luo, J. Y., Meng, M., Yao, J. S., Li, X. G., Zha, Y. Q., Wang, X. T. et al., 2009. One-step synthesis of nanostructured Pd-doped mixed oxides MOx-CeO_2 (M = Mn, Fe, Co, Ni, Cu) for efficient CO and C_3H_8 total oxidation. Appl. Catal. B 87, 92–103.

Martínez, A. A., Fernández, M. G., Hungría, A. B., Iglesias, J., Duncan, K., Smith, R. et al., 2001. Effect of thermal sintering on light-off performance of Pd/(Ce, Zr)O*x*/Al_2O_3 three-way catalysts: Model gas and engine tests. J. Catal. 204(1), 238–248.

Martínez-Arias, A., Fernández-García, M., Iglesias-Juez, A., Hungría, A. B., Anderson, J. A., Conesa, J. C. et al., 2001. New Pd/CexZr1 – $x$$O_2$/$Al_2O_3$ three-way catalysts prepared by microemulsion Part 2. In situ analysis of CO oxidation and NO reduction under stoichiometric CO+NO+CO_2. Appl. Catal. B. 31, 51–60.

Matsumoto, S., 2004. Recent advances in automobile exhaust catalysts. Catal. Today 90(3-4), 183–190.

Morikawa, A., Suzuki, T., Kanazawa, T., Kikuta, K., Suda, A., Shinjo, H., 2008. A new concept in high performance ceria-zirconia oxygen storage capacity material with Al_2O_3 as a diffusion barrier. Appl. Catal. B 78(3-4), 210–221.

Nagai, Y., Dohmae, K., Ikeda, Y., Takagi, N., Tanabe, T., Hara, N. et al., 2008. In situ redispersion of platinum autoexhaust catalysts: An online approach to increasing catalyst lifetimes? Angew. Chem. Inter. Ed 47(48), 9303–9306.

Nagai, Y., Hirabayashi, T., Dohmae, K., Takagi, N., Minami, T., Shinjoh, H. et al., 2006. Sintering inhibition mechanism of platinum supported on ceria-based oxideand Pt-oxide-support interaction. J. Catal. 242(1), 103–109.

Nishihata, Y., Mizuki, J., Akao, T., Tanaka, H., Uenishi, M., Kimura, M. et al., 2002. Self-regeneration of a Pd-perovskite catalyst for automotive emissions control. Nature 418(6894), 164–167.

Papavasiliou, A., Tsetsekou, A., Matsouka, V., Konsolakis, M., Yentekakis, I. V., Boukos, N., 2009. Development of a Ce-Zr-La modified Pt/γ-Al_2O_3 TWCs washcoat: effect of synthesis procedure on catalytic behavior and thermal durability. Appl. Catal. B. 90(1-2), 162–174.

Parks, G. A., 1965. The iso-electric points of solid oxides, solid hydroxides, and aqueous hydroxo complex systems. Chem. Rev. 65(2), 177–198.

Qiao, B. T., Wang, A. Q., Yang, X. F., Allard, L. F., Jiang, Z., Cui, Y. T. et al., 2011. Single-atom catalysis of CO oxidation using Pt1/FeOx. Nature Chem. 3(8), 634–641.

Shelef, M., McCabe, R. W., 2000. Twenty-five years after introduction of automotive catalysts: what next? Catal. Today 62(1-2), 35–50.

Shinjoh, H., Hatanaka, M., Nagai, Y., Tanabe, T., Takahashi, N., Yoshida, T. et al., 2009. Suppression of noble metal sintering based on the support anchoring effect and its application in automotive three-way catalysis. Topic in Catal. 52(13-20), 1967–1971.

Singh, P., Hegde, M. S., 2010. Sono-chemical synthesis of thermally stable hierarchical $Ce_{1-x}M_xO_{2-\delta}$ (M=Pt or Pd, $0 \leqslant x \leqslant 0.10$) nano-crystallites: Redox properties and methanol electro-oxidation activity. Crystal Growth and Design 10: 2995–3004.

Terribile, D., Trovarelli, A., Llorca, J., Leitenburg, C. D., Dolcetti, G., 1998. The synthesis and characterization of mesoporous high-surface area ceria prepared using a hybrid organic/inorganic route. J. Catal. 178(1), 299–308.

Wang, Q. Y., Zhao, B., Li, G. F., Zhou, R. X., 2011. Effect of synthesis method on the properties of ceria-zirconia modified alumina and the catalytic performance of its supported Pd-only three-way catalyst. J. Molec. Catal. A 344(1-2), 132–137.

Wei, Y. C., Liu, J., Zhao, Z., Chen, Y. S., Xu, C. M., Duan, A. J. et al., 2011a. Highly active catalysts of gold nanoparticles supported on three-dimensionally ordered macroporous $LaFeO_3$ for soot oxidation. Angew. Chem. Int. Ed. 50(10), 2326–2329.

Wei, Y. C., Liu, J., Zhao, Z., Duan, A. J., Jiang, G. Y., Xu, C. M. et al., 2011b. Three-dimensionally ordered macroporous Ce0.8Zr0.2O_2-supported gold nanoparticles: synthesis with controllable size and super-catalytic performance for soot oxidation. Energy Environ. Sci. 4(8), 2959–2970.

Williamson, W. B., Perry, J., Gandhi, H. S., Bomback, J. L., 1985. Effects of oil phosphorus on deactivation of monolithic three-way catalysts. Appl. Catal. 15(2), 277–292.